Charge separation measurements in $p(d)$+Au and Au+Au collisions; implications for the chiral magnetic effect

J. Adam,[6] L. Adamczyk,[2] J. R. Adams,[39] J. K. Adkins,[30] G. Agakishiev,[28] M. M. Aggarwal,[41] Z. Ahammed,[61] I. Alekseev,[3,35] D. M. Anderson,[55] A. Aparin,[28] E. C. Aschenauer,[6] M. U. Ashraf,[11] F. G. Atetalla,[29] A. Attri,[41] G. S. Averichev,[28] V. Bairathi,[53] K. Barish,[10] A. Behera,[52] R. Bellwied,[20] A. Bhasin,[27] J. Bielcik,[14] J. Bielcikova,[38] L. C. Bland,[6] I. G. Bordyuzhin,[3] J. D. Brandenburg,[49,6] A. V. Brandin,[35] J. Butterworth,[45] H. Caines,[64] M. Calderón de la Barca Sánchez,[8] D. Cebra,[8] I. Chakaberia,[29,6] P. Chaloupka,[14] B. K. Chan,[9] F-H. Chang,[37] Z. Chang,[6] N. Chankova-Bunzarova,[28] A. Chatterjee,[11] D. Chen,[10] J. H. Chen,[18] X. Chen,[48] Z. Chen,[49] J. Cheng,[57] M. Cherney,[13] M. Chevalier,[10] S. Choudhury,[18] W. Christie,[6] X. Chu,[6] H. J. Crawford,[7] M. Csanád,[16] M. Daugherity,[1] T. G. Dedovich,[28] I. M. Deppner,[19] A. A. Derevschikov,[43] L. Didenko,[6] X. Dong,[31] J. L. Drachenberg,[1] J. C. Dunlop,[6] T. Edmonds,[44] N. Elsey,[63] J. Engelage,[7] G. Eppley,[45] R. Esha,[52] S. Esumi,[58] O. Evdokimov,[12] A. Ewigleben,[32] O. Eyser,[6] R. Fatemi,[30] S. Fazio,[6] P. Federic,[38] J. Fedorisin,[28] C. J. Feng,[37] Y. Feng,[44] P. Filip,[28] E. Finch,[51] Y. Fisyak,[6] A. Francisco,[64] L. Fulek,[2] C. A. Gagliardi,[55] T. Galatyuk,[15] F. Geurts,[45] A. Gibson,[60] K. Gopal,[23] D. Grosnick,[60] W. Guryn,[6] A. I. Hamad,[29] A. Hamed,[5] S. Harabasz,[15] J. W. Harris,[64] S. He,[11] W. He,[18] X. He,[26] S. Heppelmann,[8] S. Heppelmann,[42] N. Herrmann,[19] E. Hoffman,[20] L. Holub,[14] Y. Hong,[31] S. Horvat,[64] Y. Hu,[18] H. Z. Huang,[9] S. L. Huang,[52] T. Huang,[37] X. Huang,[57] T. J. Humanic,[39] P. Huo,[52] G. Igo,[9] D. Isenhower,[1] W. W. Jacobs,[25] C. Jena,[23] A. Jentsch,[6] Y. JI,[48] J. Jia,[6,52] K. Jiang,[48] S. Jowzaee,[63] X. Ju,[48] E. G. Judd,[7] S. Kabana,[53] M. L. Kabir,[10] S. Kagamaster,[32] D. Kalinkin,[25] K. Kang,[57] D. Kapukchyan,[10] K. Kauder,[6] H. W. Ke,[6] D. Keane,[29] A. Kechechyan,[28] M. Kelsey,[31] Y. V. Khyzhniak,[35] D. P. Kikoła,[62] C. Kim,[10] B. Kimelman,[8] D. Kincses,[16] T. A. Kinghorn,[8] I. Kisel,[17] A. Kiselev,[6] A. Kisiel,[62] M. Kocan,[14] L. Kochenda,[35] L. K. Kosarzewski,[14] L. Kramarik,[14] P. Kravtsov,[35] K. Krueger,[4] N. Kulathunga Mudiyanselage,[20] L. Kumar,[41] R. Kunnawalkam Elayavalli,[63] J. H. Kwasizur,[25] R. Lacey,[52] S. Lan,[11] J. M. Landgraf,[6] J. Lauret,[6] A. Lebedev,[6] R. Lednicky,[28] J. H. Lee,[6] Y. H. Leung,[31] C. Li,[48] W. Li,[50] W. Li,[45] X. Li,[48] Y. Li,[57] Y. Liang,[29] R. Licenik,[38] T. Lin,[55] Y. Lin,[11] M. A. Lisa,[39] F. Liu,[11] H. Liu,[25] P. Liu,[52] P. Liu,[50] T. Liu,[64] X. Liu,[39] Y. Liu,[55] Z. Liu,[48] T. Ljubicic,[6] W. J. Llope,[63] R. S. Longacre,[6] N. S. Lukow,[54] S. Luo,[12] X. Luo,[11] G. L. Ma,[50] L. Ma,[18] R. Ma,[6] Y. G. Ma,[50] N. Magdy,[12] R. Majka,[64] D. Mallick,[36] S. Margetis,[29] C. Markert,[56] H. S. Matis,[31] J. A. Mazer,[46] N. G. Minaev,[43] S. Mioduszewski,[55] B. Mohanty,[36] M. M. Mondal,[52] I. Mooney,[63] Z. Moravcova,[14] D. A. Morozov,[43] M. Nagy,[16] J. D. Nam,[54] Md. Nasim,[22] K. Nayak,[11] D. Neff,[9] J. M. Nelson,[7] D. B. Nemes,[64] M. Nie,[49] G. Nigmatkulov,[35] T. Niida,[58] L. V. Nogach,[43] T. Nonaka,[58] A. S. Nunes,[6] G. Odyniec,[31] A. Ogawa,[6] S. Oh,[31] V. A. Okorokov,[35] B. S. Page,[6] R. Pak,[6] A. Pandav,[36] Y. Panebratsev,[28] B. Pawlik,[40] D. Pawlowska,[62] H. Pei,[11] C. Perkins,[7] L. Pinsky,[20] R. L. Pintér,[16] J. Pluta,[62] J. Porter,[31] M. Posik,[54] N. K. Pruthi,[41] M. Przybycien,[2] J. Putschke,[63] H. Qiu,[26] A. Quintero,[54] S. K. Radhakrishnan,[29] S. Ramachandran,[30] R. L. Ray,[56] R. Reed,[32] H. G. Ritter,[31] J. B. Roberts,[45] O. V. Rogachevskiy,[28] J. L. Romero,[8] L. Ruan,[6] J. Rusnak,[38] N. R. Sahoo,[49] H. Sako,[58] S. Salur,[46] J. Sandweiss,[64] S. Sato,[58] W. B. Schmidke,[6] N. Schmitz,[33] B. R. Schweid,[52] F. Seck,[15] J. Seger,[13] M. Sergeeva,[9] R. Seto,[10] P. Seyboth,[33] N. Shah,[24] E. Shahaliev,[28] P. V. Shanmuganathan,[6] M. Shao,[48] F. Shen,[49] W. Q. Shen,[50] S. S. Shi,[11] Q. Y. Shou,[50] E. P. Sichtermann,[31] R. Sikora,[2] M. Simko,[38] J. Singh,[41] S. Singha,[26] N. Smirnov,[64] W. Solyst,[25] P. Sorensen,[6] H. M. Spinka,[4] B. Srivastava,[44] T. D. S. Stanislaus,[60] M. Stefaniak,[62] D. J. Stewart,[64] M. Strikhanov,[35] B. Stringfellow,[44] A. A. P. Suaide,[47] M. Sumbera,[38] B. Summa,[42] X. M. Sun,[11] X. Sun,[12] Y. Sun,[48] Y. Sun,[21] B. Surrow,[54] D. N. Svirida,[3] P. Szymanski,[62] A. H. Tang,[6] Z. Tang,[48] A. Taranenko,[35] T. Tarnowsky,[34] J. H. Thomas,[31] A. R. Timmins,[20] D. Tlusty,[13] M. Tokarev,[28] C. A. Tomkiel,[32] S. Trentalange,[9] R. E. Tribble,[55] P. Tribedy,[6] S. K. Tripathy,[16] O. D. Tsai,[9] Z. Tu,[6] T. Ullrich,[6] D. G. Underwood,[4] I. Upsal,[49,6] G. Van Buren,[6] J. Vanek,[38] A. N. Vasiliev,[43] I. Vassiliev,[17] F. Videbæk,[6] S. Vokal,[28] S. A. Voloshin,[63] F. Wang,[44] G. Wang,[9] J. S. Wang,[21] P. Wang,[48] Y. Wang,[11] Y. Wang,[57] Z. Wang,[49] J. C. Webb,[6] P. C. Weidenkaff,[19] L. Wen,[9] G. D. Westfall,[34] H. Wieman,[31] S. W. Wissink,[25] R. Witt,[59] Y. Wu,[10] Z. G. Xiao,[57] G. Xie,[31] W. Xie,[44] H. Xu,[21] N. Xu,[31] Q. H. Xu,[49] Y. F. Xu,[50] Y. Xu,[49] Z. Xu,[6] Z. Xu,[9] C. Yang,[49] Q. Yang,[49] S. Yang,[6] Y. Yang,[37] Z. Yang,[11] Z. Ye,[45] Z. Ye,[12] L. Yi,[49] K. Yip,[6] H. Zbroszczyk,[62] W. Zha,[48] D. Zhang,[11] S. Zhang,[48] S. Zhang,[50] X. P. Zhang,[57] Y. Zhang,[48] Y. Zhang,[11] Z. J. Zhang,[37] Z. Zhang,[6] Z. Zhang,[12] J. Zhao,[44] C. Zhong,[50] C. Zhou,[50] X. Zhu,[57] Z. Zhu,[49] M. Zurek,[31] and M. Zyzak[17]

(STAR Collaboration)

arXiv:2006.04251v1 [nucl-ex] 7 Jun 2020

[1] *Abilene Christian University, Abilene, Texas 79699*
[2] *AGH University of Science and Technology, FPACS, Cracow 30-059, Poland*
[3] *Alikhanov Institute for Theoretical and Experimental Physics NRC "Kurchatov Institute", Moscow 117218, Russia*
[4] *Argonne National Laboratory, Argonne, Illinois 60439*
[5] *American University of Cairo, New Cairo 11835, New Cairo, Egypt*
[6] *Brookhaven National Laboratory, Upton, New York 11973*
[7] *University of California, Berkeley, California 94720*
[8] *University of California, Davis, California 95616*
[9] *University of California, Los Angeles, California 90095*
[10] *University of California, Riverside, California 92521*
[11] *Central China Normal University, Wuhan, Hubei 430079*
[12] *University of Illinois at Chicago, Chicago, Illinois 60607*
[13] *Creighton University, Omaha, Nebraska 68178*
[14] *Czech Technical University in Prague, FNSPE, Prague 115 19, Czech Republic*
[15] *Technische Universität Darmstadt, Darmstadt 64289, Germany*
[16] *ELTE Eötvös Loránd University, Budapest, Hungary H-1117*
[17] *Frankfurt Institute for Advanced Studies FIAS, Frankfurt 60438, Germany*
[18] *Fudan University, Shanghai, 200433*
[19] *University of Heidelberg, Heidelberg 69120, Germany*
[20] *University of Houston, Houston, Texas 77204*
[21] *Huzhou University, Huzhou, Zhejiang 313000*
[22] *Indian Institute of Science Education and Research (IISER), Berhampur 760010 , India*
[23] *Indian Institute of Science Education and Research (IISER) Tirupati, Tirupati 517507, India*
[24] *Indian Institute Technology, Patna, Bihar 801106, India*
[25] *Indiana University, Bloomington, Indiana 47408*
[26] *Institute of Modern Physics, Chinese Academy of Sciences, Lanzhou, Gansu 730000*
[27] *University of Jammu, Jammu 180001, India*
[28] *Joint Institute for Nuclear Research, Dubna 141 980, Russia*
[29] *Kent State University, Kent, Ohio 44242*
[30] *University of Kentucky, Lexington, Kentucky 40506-0055*
[31] *Lawrence Berkeley National Laboratory, Berkeley, California 94720*
[32] *Lehigh University, Bethlehem, Pennsylvania 18015*
[33] *Max-Planck-Institut für Physik, Munich 80805, Germany*
[34] *Michigan State University, East Lansing, Michigan 48824*
[35] *National Research Nuclear University MEPhI, Moscow 115409, Russia*
[36] *National Institute of Science Education and Research, HBNI, Jatni 752050, India*
[37] *National Cheng Kung University, Tainan 70101*
[38] *Nuclear Physics Institute of the CAS, Rez 250 68, Czech Republic*
[39] *Ohio State University, Columbus, Ohio 43210*
[40] *Institute of Nuclear Physics PAN, Cracow 31-342, Poland*
[41] *Panjab University, Chandigarh 160014, India*
[42] *Pennsylvania State University, University Park, Pennsylvania 16802*
[43] *NRC "Kurchatov Institute", Institute of High Energy Physics, Protvino 142281, Russia*
[44] *Purdue University, West Lafayette, Indiana 47907*
[45] *Rice University, Houston, Texas 77251*
[46] *Rutgers University, Piscataway, New Jersey 08854*
[47] *Universidade de São Paulo, São Paulo, Brazil 05314-970*
[48] *University of Science and Technology of China, Hefei, Anhui 230026*
[49] *Shandong University, Qingdao, Shandong 266237*
[50] *Shanghai Institute of Applied Physics, Chinese Academy of Sciences, Shanghai 201800*
[51] *Southern Connecticut State University, New Haven, Connecticut 06515*
[52] *State University of New York, Stony Brook, New York 11794*
[53] *Instituto de Alta Investigación, Universidad de Tarapacá, Chile*
[54] *Temple University, Philadelphia, Pennsylvania 19122*
[55] *Texas A&M University, College Station, Texas 77843*
[56] *University of Texas, Austin, Texas 78712*
[57] *Tsinghua University, Beijing 100084*
[58] *University of Tsukuba, Tsukuba, Ibaraki 305-8571, Japan*
[59] *United States Naval Academy, Annapolis, Maryland 21402*
[60] *Valparaiso University, Valparaiso, Indiana 46383*
[61] *Variable Energy Cyclotron Centre, Kolkata 700064, India*
[62] *Warsaw University of Technology, Warsaw 00-661, Poland*
[63] *Wayne State University, Detroit, Michigan 48201*
[64] *Yale University, New Haven, Connecticut 06520*

Charge separation (ΔS) measurements, obtained relative to the 2$^{\rm nd}$-order (Ψ_2) and 3$^{\rm rd}$-order (Ψ_3) event planes with a new charge-sensitive correlator $R_{\Psi_m}(\Delta S)$, are presented for $p(d)$+Au and Au+Au collisions at $\sqrt{s_{NN}}$ = 200 GeV. The correlator, which is sensitive to the hypothesized Chiral Magnetic Effect (CME), show the expected patterns of background-driven charge separation for the measurements relative to Ψ_3 and those relative to Ψ_2 for the $p(d)$+Au systems. By contrast, the Au+Au measurements relative to Ψ_2, show event-shape-independent $R_{\Psi_2}(\Delta S)$ distributions consistent with a CME-driven charge separation, quantified by widths having an inverse relationship to the Fourier dipole coefficient $\tilde{a}_1$, which evaluates the CME. The extracted values of these widths and their dependencies on centrality and event-shape give new constraints for a possible CME-driven charge separation in relativistic heavy ion collisions.

PACS numbers: Valid PACS appear here

Topological charge fluctuations [1] can lead to the formation of metastable domains with a chirality imbalance, in which fundamental symmetries ($\mathcal{P}$ and/or $\mathcal{CP}$) are locally broken [2]. It has been predicted [3] that experimental manifestations of such fluctuations, as well as information on the restoration of chiral symmetry, are accessible via studies of the Chiral Magnetic Effect (CME) [3–11] in quark gluon plasma (QGP) created in the presence of the very strong magnetic fields produced in ion-ion collisions. The CME results from anomalous transport of chiral fermions in the QGP, leading to the generation of an electric current $\vec{J}_Q = \sigma_5 \vec{B}$ along the generated time-dependent magnetic field $\vec{B}$. Here, $\sigma_5 = C_A \mu_5$ is the chiral magnetic conductivity [12], expressed in terms of the chiral chemical potential μ_5 that quantifies the imbalance between right-handed and left-handed (opposite chirality) quarks in the plasma, and the coefficient $C_A = Q^2/(4\pi^2)$ for quark electric charge Q [7, 13–15]. The lifetime of the magnetic field, as well as the initial chiral imbalance and its lifetime, are currently unconstrained theoretically [16–18].

In ion-ion collisions, the CME manifests as a charge separation/asymmetry in the distribution of particles emitted about the reaction plane ($\Psi_{\rm RP}$) defined by the impact parameter and the beam axis. This asymmetry results from the B-field-driven anomalous electric current $\vec{J}_Q$ along the magnetic field direction, i.e., perpendicular to $\Psi_{\rm RP}$. Such a charge separation leads to a dipole term (a_1) in the azimuthal distribution of the produced charged hadrons $N^{\rm ch}$:

$$\frac{dN^{\rm ch}}{d\phi} \propto [1 + 2\sum_n (v_n \cos(n\Delta\phi) + a_n \sin(n\Delta\phi))] \quad (1)$$

where $\Delta\phi = \phi - \Psi_{\rm RP}$ is the azimuthal angle measured with respect to the reaction plane angle, and v_n and a_n denote the coefficients of P-even and P-odd Fourier terms, respectively. A direct measurement of the P-odd coefficients a_n, is not possible due to the strict global $\mathcal{P}$ and $\mathcal{CP}$ symmetry of QCD. However, their fluctuation and/or variance $\tilde{a}_n = \left\langle a_n^2 \right\rangle^{1/2}$ can be measured with suitable correlators.

Several measurements have been performed at RHIC [19–23] and the LHC [24–27] to identify and quantify charge separation with the Gamma correlator [28]:

$$\gamma_{\alpha\beta} = \left\langle \cos\left(\phi_\alpha^{(\pm)} + \phi_\beta^{(\pm)} - 2\Psi_2\right) \right\rangle, \quad (2)$$

where ϕ_α, ϕ_β denote the azimuthal emission angles for like-sign and unlike-sign hadron pairs, and Ψ_2 denotes the estimated second-order event plane determined via the maximal particle density in the elliptic azimuthal anisotropy and the beam axis. The interpretation of these data as an indication for the CME-driven charge separation remains inconclusive because of the difficulty to separate the desired signal from several known sources of background correlations [29–35]. The sensitivity of the γ-correlator to local charge conservation and flow-driven background poses significant challenges for its use to identify and characterize a possible CME signal.

An alternative charge-sensitive correlator, designed to have different sensitivities to the CME signal and known backgrounds, has been proposed [36, 37] to aid the detection and characterization of CME-driven charge separation. Here, we report new measurements relative to both the Ψ_2 and Ψ_3 event planes in Au+Au and $p(d)$+Au collisions, obtained with this correlator. The measurements relative to Ψ_3, as well as those relative to Ψ_2 for the $p(d)$+Au systems, provide important benchmarks for validation and quantification of a possible CME-driven signal in Au+Au collisions. That is, there is little, if any, correlation between $\Psi_{\rm RP}$ and Ψ_3 which renders the measurements relative to Ψ_3 insensitive to CME-driven charge separation, but not necessarily to the background. Similarly, CME-driven charge separation is expected to be small, if at all present, in $p(d)$+Au collisions, due to the reduced magnetic field strength and the approximately random $\vec{B}$-field orientations (relative to both Ψ_2 and Ψ_3) in these collisions.

The data presented in this work are from $p(d)$+Au and Au+Au collisions collected at the collision energy $\sqrt{s_{\rm NN}} = 200$ GeV with the STAR detector using a minimum bias trigger [38]. Charged-particle tracks, measured in the full azimuth and the pseudorapidity range $|\eta| < 1.0$ of the Time Projection Chamber (TPC) [39], were used to reconstruct the collision vertices. Events were selected with vertex positions within $\pm$30 cm from the nominal center of the TPC (in the beam direction), and within

± 2 cm in the radial direction with respect to the center of the beam.

The centrality of each collision was determined by measuring event-by-event multiplicity and interpreting the measurement with a tuned Monte Carlo Glauber calculation [40]. Analyzed tracks were required to have a distance of closest approach (DCA) to the primary vertex of less than 3 cm, and to have at least 15 TPC space points used in their reconstruction. Furthermore, the ratio of the number of fit points to the maximum possible number of TPC space points was required to be larger than 0.52 to remove the effects of split and merged tracks.

The $R_{\Psi_m}(\Delta S)$ correlators employed in our analysis, are obtained from the ratio of two sets of correlation functions [36, 37];

$$R_{\Psi_m}(\Delta S) = C_{\Psi_m}(\Delta S)/C^{\perp}_{\Psi_m}(\Delta S),\ m = 2, 3, ..., \quad (3)$$

where $C_{\Psi_m}(\Delta S)$ and $C^{\perp}_{\Psi_m}(\Delta S)$ are used to quantify charge separation ΔS, perpendicular and parallel (respectively) to the Ψ_m event planes. For Ψ_2, these correlation functions measure charge separation parallel and perpendicular (respectively) to the $\vec{B}$-field. Both were constructed from the ratio of two distributions, following the procedure outlined in Refs. [36, 37];

$$C_{\Psi_m}(\Delta S) = \frac{N_{\rm real}(\Delta S)}{N_{\rm shuffled}(\Delta S)}, \quad (4)$$

where $N_{\rm real}(\Delta S)$ is the distribution over events of the event-by-event average of the charge separation;

$$\Delta S = \frac{\sum_1^{n^+} w_i^+ \sin(\frac{m}{2}\Delta\varphi_m)}{\sum_1^{n^+} w_i^+} - \frac{\sum_1^{n^-} w_i^- \sin(\frac{m}{2}\Delta\varphi_m)}{\sum_1^{n^-} w_i^-}, \quad (5)$$

where n^- and n^+ are the numbers of negatively and positively charged particles emitted about the estimated Ψ_m planes, $w_i^{\pm}$ are weights which take account of the azimuthal acceptance for positively and negatively charged particles, and $\Delta\varphi_m = \phi - \Psi_m$. The $N_{\rm shuffled}(\Delta S)$ distribution was obtained via random reassignment (shuffling) of the charges of the reconstructed tracks in each event. This procedure ensures identical event-by-event properties for the numerator and the denominator in Eq. 4, except for the sensitivity to charge-dependent correlations that is fully removed in the denominator. The $N_{\rm real}(\Delta S)$ and $N_{\rm shuffled}(\Delta S)$ distributions used to construct $C^{\perp}_{\Psi_m}(\Delta S)$, were obtained from the same events used to construct $C_{\Psi_m}(\Delta S)$, but with Ψ_m replaced by $\Psi_m + \pi/m$ to ensure that only background-driven charge separation contributes to $C^{\perp}_{\Psi_m}(\Delta S)$. The ratios $N_{\rm real}(\Delta S)/N_{\rm shuffled}(\Delta S)$ yield Gaussian distributions for both $C_{\Psi_m}(\Delta S)$ and $C^{\perp}_{\Psi_m}(\Delta S)$.

The correlator $R_{\Psi_2}(\Delta S) = C_{\Psi_2}(\Delta S)/C^{\perp}_{\Psi_2}(\Delta S)$, is designed to measure the magnitude of charge separation parallel to the $\vec{B}$-field, relative to that for charge separation perpendicular to the $\vec{B}$-field. Since the CME drives charge separation along the $\vec{B}$-field, it is expected to lead to concave-shaped $R_{\Psi_2}(\Delta S)$ distributions [36] having widths that reflect the magnitude $\tilde{a}_1$ of the charge separation (cf. Eq. 1). By contrast, the correlator $R_{\Psi_3}(\Delta S) = C_{\Psi_3}(\Delta S)/C^{\perp}_{\Psi_3}(\Delta S)$ is insensitive to a CME-driven charge separation, due to the very weak correlation between the orientation of Ψ_3 and the $\vec{B}$-field. Thus, the identification and characterization of CME-driven charge separation requires both a concave-shaped distribution for $R_{\Psi_2}(\Delta S)$ and an observed difference between the distributions for $R_{\Psi_2}(\Delta S)$ and $R_{\Psi_3}(\Delta S)$ [36, 37], i.e, a concave-shaped $R_{\Psi_2}(\Delta S)$ distribution is necessary but insufficient for signal identification and characterization. An important corollary signaling the dominance of background-driven charge separation, is a characteristically similar pattern (in magnitude and trend) for the $R_{\Psi_2}(\Delta S)$ and $R_{\Psi_3}(\Delta S)$ correlators [36], as demonstrated in Fig. 1(a) and further discussed below. This similarity is to be expected regardless of whether or not the background-driven distribution for $R_{\Psi_3}(\Delta S)$ is convex- or concave-shaped [36, 41].

The magnitude of the charge separation is reflected in the widths of the concave-shaped distributions for $R_{\Psi_2}(\Delta S)$, which are also influenced by particle number fluctuations and the resolution of Ψ_2. That is, stronger CME-driven signals lead to narrower concave-shaped distributions (smaller widths), which are made broader by particle number fluctuations and poorer event-plane resolutions. The influence of particle number fluctuations can be mitigated by scaling ΔS by the width $\sigma_{\Delta_{\rm Sh}}$ of the distribution for $N_{\rm shuffled}(\Delta S)$ i.e., $\Delta S^{'} = \Delta S/\sigma_{\Delta_{\rm Sh}}$. Similarly, the effects of the event plane resolution can be taken into account by scaling $\Delta S^{'}$ by the parametrized resolution factor $\delta_R = {\rm Res} \cdot e^{(1-{\rm Res})^2}$, i.e., $\Delta S^{''} = \Delta S^{'} \cdot \delta_R$, where Res is the event plane resolution. The efficacy of both scaling factors has been confirmed via detailed simulation studies, as well as with data-driven tests.

For the present analysis, charged particles with transverse momentum $0.2 < p_T < 2.0$ GeV/c were used to construct Ψ_2 and Ψ_3. For Au+Au collisions, each event was subdivided into two sub-events with pseudorapidity $0.1 < \eta < 1.0$ (West) and $-1.0 < \eta < -0.1$ (East) to obtain $\Psi_m^{\rm E}$ (East) and $\Psi_m^{\rm W}$ (West); the associated centrality-dependent event-plane resolution factors are comparable to those reported in Ref. [42]. For $p(d)$+Au collisions, Ψ_m was determined only in the Au going direction; the associated event-plane resolution factors for Ψ_2 in central p+Au and d+Au collisions ($\langle N_{\rm ch}\rangle = 20 \pm 3$) are 0.184 and 0.263 respectively. They can be compared to the value 0.346, extracted for peripheral Au+Au collisions of similar $\langle N_{\rm ch}\rangle$. Subsequently, $C_{\Psi_m}(\Delta S)$, $C^{\perp}_{\Psi_m}(\Delta S)$ and $R_{\Psi_m}(\Delta S)$ were determined for charged particles with $0.35 < p_T < 2.0$ GeV/c, taking care to use $\Psi_m^{\rm W}$ for particles within the range $0.1 < \eta < 1.0$ and $\Psi_m^{\rm E}$ for particles

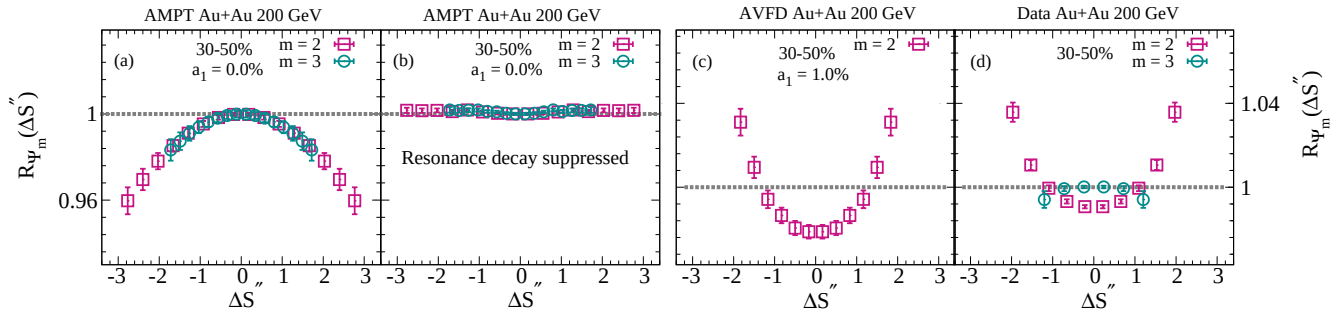

FIG. 1. Comparison of the $R_{\Psi_m}(\Delta S^{''})$ distributions for charged particles in Au+Au collisions ($\sqrt{s_{NN}} = 200$ GeV). Results are shown for (a) purely background-driven charge separation for 30-50% central events obtained with the AMPT model; (b) same as (a) but with resonance decays suppressed; (c) the combined effects of background- and CME-driven ($\tilde{a}_1 = 1.0\%$) charge separation obtained for 30-50% central events with the AVFD model and (d) data for 30-50% central events from this study.

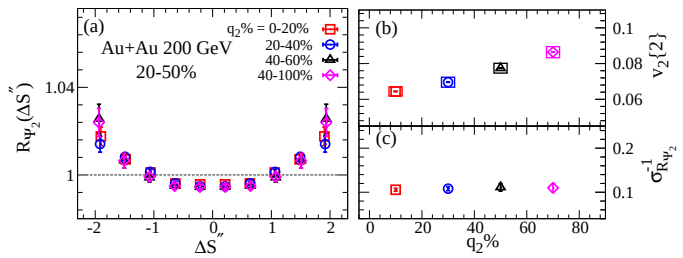

FIG. 2. (a) Comparison of the $R_{\Psi_2}(\Delta S^{''})$ correlators for q_2 selected events in $20-50\%$ central, Au+Au collisions at $\sqrt{s_{\rm NN}} = 200$ GeV; (b) $v_2(q_2)$ vs. q_2 for the same q_2-selected events; (c) comparison of the inverse widths $\sigma^{-1}_{R_{\Psi_2}}$ for the $R_{\Psi_2}(\Delta S^{''})$ distributions shown in panel (a).

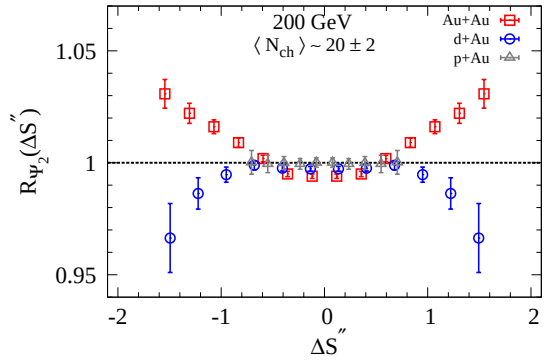

FIG. 3. Comparison of the $R_{\Psi_2}(\Delta S^{''})$ correlators obtained for charged particles in peripheral Au+Au and central $p(d)$+Au collisions ($\langle N_{\rm ch}\rangle \sim 20$) at $\sqrt{s_{\rm NN}} = 200$ GeV.

within the range $-1.0 < \eta < -0.1$, to avoid possible self-correlations. The latter p_T cut was chosen to minimize the influence of acceptance effects at low p_T while optimizing the statistics.

The values of $R_{\Psi_m}(\Delta S)$ were obtained for central $p(d)$+Au collisions and for Au+Au collisions at several centralities at $\sqrt{s_{\rm NN}} = 200$ GeV; note that the statistics for $p(d)$+Au collisions precluded the extraction of $R_{\Psi_3}(\Delta S)$ for these systems. Representative distributions are shown in Figs. 1(d), 2, 3 and 4. The systematic uncertainties associated with these extractions were estimated from variations in the extracted values of $R_{\Psi_m}(\Delta S)$ after varying the vertex position, DCA and $|\Delta\eta|$ over the ranges ±30 cm, 2-3 cm and 0.2-0.6 respectively. The resulting relative uncertainties which roughly cancel (cf. Eq. 3), are much smaller than the statistical uncertainties and do not exceed 1%.

To aid the interpretation of the experimental measurements, $R_{\Psi_m}(\Delta S)$ correlators were similarly obtained [36] for Au+Au collisions simulated with the Multi-Phase Transport (AMPT) Model (v1.26t5-v2.26t5) [43] and the first generation Anomalous Viscous Fluid Dynamics (AVFD) model [9]; the latter does not incorporate event-by-event fluctuations but the former does. Both models include flow and resonance decays, but do not incorporate Local charge conservation (LCC) as a background. This LCC background can influence both the magnitude and the shape of the $R_{\Psi_2}(\Delta S)$ and the $R_{\Psi_3}(\Delta S)$ correlators [36, 41], depending on its precise nature. However, it can be discerned from CME-driven charge separation via a comparison of $R_{\Psi_2}(\Delta S)$ and $R_{\Psi_3}(\Delta S)$ [36, 41] as discussed earlier. The simulated correlators, shown in Figs. 1(a)-(c), provide insight, as well as important benchmarks for qualitative comparisons between the measured correlators and those simulated for background- and background plus CME-driven charge separation.

The AMPT results shown in Fig. 1(a) indicates that, for background-driven charge separation ($a_1 = 0$), similar magnitudes and widths are to be expected for the $R_{\Psi_2}(\Delta S^{''})$ and $R_{\Psi_3}(\Delta S^{''})$ distributions. This similarity, albeit with different shaped correlators, is borne out in hydrodynamical model calculations which incorporates the LCC background [41]. Fig. 1(b) shows that the suppression of resonance decays in the AMPT events (by switching them off), results in relatively flat distributions for $R_{\Psi_m}(\Delta S^{''})$, confirming that, in the absence of resonance decays, $R_{\Psi_2}(\Delta S^{''})$ is insensitive to the background which results from flow fluctuations. This response contrasts with that for the γ correlator [34, 35]. Fig. 1(c) shows that the introduction of an input CME signal ($a_1 = 1.0\%$) in single-shot AVFD events, leads to

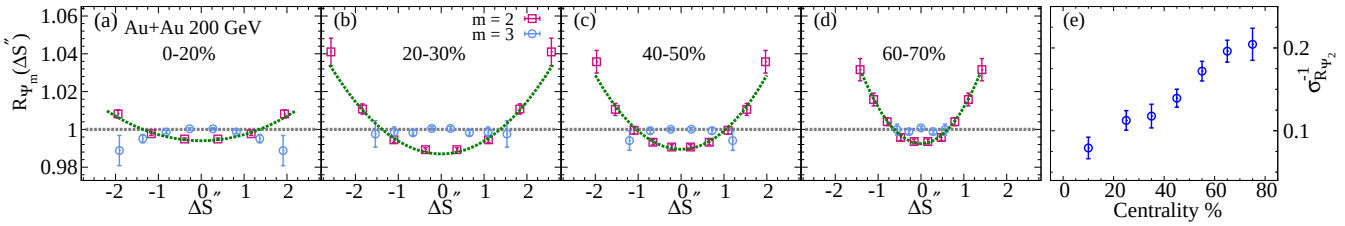

FIG. 4. Comparison of the $R_{\Psi_{2,3}}(\Delta S^{''})$ correlators obtained for charged particles in (a) $0-20\%$, (b) $20-30\%$, (c) $40-50\%$ and (d) $60-70\%$ central Au+Au collisions at $\sqrt{s_{\rm NN}} = 200$ GeV. The dashed curves represent Gaussian fits to $R_{\Psi_2}(\Delta S^{''})$ (see text). (e) Centrality dependence of the inverse widths $\sigma^{-1}_{R_{\Psi_2}} \propto \tilde{a}_1$, extracted from the $R_{\Psi_2}(\Delta S^{''})$ correlators.

the concave-shaped $R_{\Psi_2}(\Delta S^{''})$ distribution expected for CME-driven charge separation along the $\vec{B}$-field.

The $R_{\Psi_{2,3}}(\Delta S^{''})$ correlators for 30-50% Au+Au collisions are shown in Fig. 1(d); they indicate characteristic patterns which contrast with the expected similarity between $R_{\Psi_2}(\Delta S^{''})$ and $R_{\Psi_3}(\Delta S^{''})$ when background-driven charge separation dominates (cf. Fig. 1(a)). That is, $R_{\Psi_3}(\Delta S^{''})$ shows a flat or slightly convex-shaped distribution analogous to the one observed in the AMPT simulations for background-driven charge separation (Figs. 1(a) and (b)), while the concave-shaped $R_{\Psi_2}(\Delta S^{''})$ distribution is analogous to the one obtained in AVFD simulations with an input CME signal (Fig. 1(c)). These observations are incompatible with the dominance of background-driven contributions.

The sensitivity of $R_{\Psi_2}(\Delta S^{''})$ to the influence of possible background contributions can be further studied with event-shape selection, via fractional cuts on the distribution of the magnitude of the q_2 flow vector [44]. Here, the rationale is that elliptic flow v_2, which is a major driver of background correlations, is strongly correlated with q_2 [26, 45]. Thus, the influence of the background correlations can be increased(decreased) by selecting on events with larger(smaller) q_2 magnitudes.

The analysis with event-shape selection was performed with three sub-events; $A[\eta < -0.3]$, $B[|\eta| < 0.3]$, and $C[\eta > 0.3]$, following the procedures outlined earlier, and with q_2 selections in sub-event B. Fig. 2 compares the q_2-selected $R_{\Psi_2}(\Delta S^{''})$ distributions (a) and v_2 values (b) obtained for 20-50% central Au+Au collisions. They indicate that while v_2 shows a sizable increase with q_2, the corresponding widths for the $R_{\Psi_2}(\Delta S^{''})$ correlators (Fig. 2(c)) show little, if any, change. This contrasts with the q_2-dependent widths observed for background-driven charge separation in AMPT simulations. Note that the B-field is a weak function of q_2 but a strong function of centrality [26]. The observed insensitivity of the data to q_2, is incompatible with a dominating influence of background-driven contributions [26] to $R_{\Psi_2}(\Delta S^{''})$.

Further benchmarking can be achieved by comparing the $R_{\Psi_2}(\Delta S^{''})$ correlators for p+Au, d+Au and Au+Au collisions at similar $\langle N_{\rm ch}\rangle \sim 20$. Note that for this value of $\langle N_{\rm ch}\rangle$, the difference between the event plane resolution for d+Au and Au+Au collisions is about 30%. The statistical significance of the data for p+Au and d+Au precluded the extraction of $R_{\Psi_3}(\Delta S^{''})$ for these systems. The convex-shaped to flat $R_{\Psi_2}(\Delta S^{''})$ distributions shown for $p(d)$+Au collisions in Fig. 3 are reminiscent of the $R_{\Psi_3}(\Delta S^{''})$ correlators observed for Au+Au collisions (cf. Fig. 1(d) and Fig. 4), and are consistent with the reduced magnetic field strength and the approximately random $\vec{B}$-field orientations [relative to Ψ_2] expected in these collisions. In contrast, the $R_{\Psi_2}(\Delta S^{''})$ correlator for Au+Au collisions, also shown in Fig. 3, is decidedly concave-shaped, which is incompatible with the dominance of background-driven charge separation indicated by $R_{\Psi_3}(\Delta S^{''})$. The observed system-dependent patterns for $R_{\Psi_2}(\Delta S^{''})$ are compatible with the dominance of background-driven charge separation in p/d+Au collisions but not in the corresponding Au+Au collisions. This contrasts with the background-dominated measurements observed with the γ correlator for similar $\langle N_{\rm ch}\rangle$ selections in p+Pb and Pb+Pb collisions [25] and in $p(d)$+Au and Au+Au collisions [45].

The $R_{\Psi_m}(\Delta S^{''})$ correlators, extracted for several centrality selections in Au+Au collisions at $\sqrt{s_{\rm NN}} = 200$ GeV, are shown in Figs. 4(a) - (d). The qualitative patterns of a convex-shaped to an essentially flat distribution for $R_{\Psi_3}(\Delta S^{''})$ and a concave-shaped distribution for $R_{\Psi_2}(\Delta S^{''})$ are similar to those shown earlier in Figs. 1(d), 2(a) and 3; the dashed curves represent Gaussian fits ($f(x) = Ae^{0.5(x/\sigma_{R_{\Psi_2}})^2}$) to these distributions. A centrality-dependent change in $\sigma_{R_{\Psi_2}}$ is apparent from the distributions. This dependence is made more transparent in Fig. 4(e) where $\sigma^{-1}_{R_{\Psi_2}} \propto \tilde{a}_1$ [for CME dominated signal] [36] is plotted vs. centrality.

The convex to flat distributions observed for $R_{\Psi_3}(\Delta S^{''})$ at all centrality intervals and the sizable $R_{\Psi_2}(\Delta S^{''})$ centrality dependence indicated in Fig. 4(e), cannot be reconciled with any of the background-driven charge separation models. Here, it is important to recall that Fig. 2(a) gives a strong indication that $R_{\Psi_2}(\Delta S^{''})$ is relatively insensitive to v_2, which also increases as collisions become more peripheral.

In summary, we have used the charge-sensitive correlators $R_{\Psi_{2,3}}(\Delta S)$, constructed relative to the 2$^{\rm nd}$ and

3rd-order event planes, to perform charge separation measurements in $p(d)$+Au and Au+Au collisions at $\sqrt{s_{\rm NN}} =$ 200 GeV. The correlators indicate convex-shaped to flat $R_{\Psi_m}(\Delta S^{''})$ distributions for the measurements relative to Ψ_3 and those relative to Ψ_2 for the $p(d)$+Au systems. In contrast, the Au+Au measurements relative to Ψ_2, show concave-shaped $R_{\Psi_2}(\Delta S^{''})$ distributions. The inverse widths of the $R_{\Psi_2}(\Delta S^{''})$ distributions, which serve to quantify the magnitude of the charge separation, show an increase from central to peripheral collisions but are insensitive to event-shape slection.

Background scenarios of flow, flow fluctuations, resonance decay and local charge conservation effects, as implemented in the AMPT [35, 46], AVFD [36], and 3+1-dimensional hydrodynamic [41] models cannot provide a simultaneous description of $R_{\Psi_{2,3}}(\Delta S)$ for Au+Au, $R_{\Psi_2}(\Delta S)$ for $p(d)$+Au, and the q_2 dependence of $R_{\Psi_2}(\Delta S)$ for Au+Au. Instead, these correlator responses suggest a distinction between background- and CME-driven charge separation, which could aid characterization of the CME. These measurements not only provide a crucial experimental test for the CME in Au+Au collisions at RHIC, but could also aid the development of a detailed understanding of the chiral and topological properties of the QGP produced in these collisions.

ACKNOWLEDGMENTS

We thank the RHIC Operations Group and RCF at BNL, the NERSC Center at LBNL, and the Open Science Grid consortium for providing resources and support. This work was supported in part by the Office of Nuclear Physics within the U.S. DOE Office of Science, the U.S. National Science Foundation, the Ministry of Education and Science of the Russian Federation, National Natural Science Foundation of China, Chinese Academy of Science, the Ministry of Science and Technology of China and the Chinese Ministry of Education, the Higher Education Sprout Project by Ministry of Education at NCKU, the National Research Foundation of Korea, Czech Science Foundation and Ministry of Education, Youth and Sports of the Czech Republic, Hungarian National Research, Development and Innovation Office, New National Excellency Programme of the Hungarian Ministry of Human Capacities, Department of Atomic Energy and Department of Science and Technology of the Government of India, the National Science Centre of Poland, the Ministry of Science, Education and Sports of the Republic of Croatia, RosAtom of Russia and German Bundesministerium fur Bildung, Wissenschaft, Forschung and Technologie (BMBF), Helmholtz Association, Ministry of Education, Culture, Sports, Science, and Technology (MEXT) and Japan Society for the Promotion of Science (JSPS).

[1] Thomas Schafer and Edward V. Shuryak, "Instantons in QCD," Rev. Mod. Phys. **70**, 323–426 (1998), arXiv:hep-ph/9610451.

[2] Dmitri E. Kharzeev, "Topologically induced local P and CP violation in QCD x QED," Annals Phys. **325**, 205–218 (2010), arXiv:0911.3715 [hep-ph].

[3] Dmitri Kharzeev, "Parity violation in hot QCD: Why it can happen, and how to look for it," Phys. Lett. **B633**, 260–264 (2006), arXiv:hep-ph/0406125.

[4] A. Vilenkin, "Equilibrium parity-violating current in a magnetic field," Phys. Rev. **D22**, 3080–3084 (1980).

[5] D. Kharzeev and A. Zhitnitsky, "Charge separation induced by P-odd bubbles in QCD matter," Nucl. Phys. **A797**, 67–79 (2007), arXiv:0706.1026 [hep-ph].

[6] Dmitri E. Kharzeev, Larry D. McLerran, and Harmen J. Warringa, "The effects of topological charge change in heavy ion collisions: 'Event by event P and CP violation'," Nucl. Phys. **A803**, 227–253 (2008), arXiv:0711.0950 [hep-ph].

[7] Kenji Fukushima, Dmitri E. Kharzeev, and Harmen J. Warringa, "The Chiral Magnetic Effect," Phys. Rev. **D78**, 074033 (2008), arXiv:0808.3382 [hep-ph].

[8] D. E. Kharzeev, J. Liao, S. A. Voloshin, and G. Wang, "Chiral magnetic and vortical effects in high-energy nuclear collisions−A status report," Prog. Part. Nucl. Phys. **88**, 1–28 (2016), arXiv:1511.04050 [hep-ph].

[9] Yin Jiang, Shuzhe Shi, Yi Yin, and Jinfeng Liao, "Quantifying the chiral magnetic effect from anomalous-viscous fluid dynamics," Chin. Phys. C **42**, 011001 (2018), arXiv:1611.04586 [nucl-th].

[10] Shuzhe Shi, Yin Jiang, Elias Lilleskov, and Jinfeng Liao, "Anomalous Chiral Transport in Heavy Ion Collisions from Anomalous-Viscous Fluid Dynamics," Annals Phys. **394**, 50–72 (2018), arXiv:1711.02496 [nucl-th].

[11] Adam Bzdak, Shinichi Esumi, Volker Koch, Jinfeng Liao, Mikhail Stephanov, and Nu Xu, "Mapping the Phases of Quantum Chromodynamics with Beam Energy Scan," Phys. Rept. **853**, 1–87 (2020), arXiv:1906.00936 [nucl-th].

[12] Dmitri E. Kharzeev and Harmen J. Warringa, "Chiral magnetic conductivity," Phys. Rev. **D80**, 034028 (2009), arXiv:0907.5007 [hep-ph].

[13] Dam T. Son and Piotr Surowka, "Hydrodynamics with Triangle Anomalies," Phys. Rev. Lett. **103**, 191601 (2009), arXiv:0906.5044 [hep-th].

[14] Valentin I. Zakharov, "Chiral Magnetic Effect in Hydrodynamic Approximation," Lect. Notes Phys. **871**, 295–330 (2013), arXiv:1210.2186 [hep-ph].

[15] Kenji Fukushima, "Views of the Chiral Magnetic Effect," Lect. Notes Phys. **871**, 241–259 (2013), arXiv:1209.5064 [hep-ph].

[16] L. McLerran and V. Skokov, "Comments About the Electromagnetic Field in Heavy-Ion Col-

lisions," Nucl. Phys. **A929**, 184–190 (2014), arXiv:1305.0774 [hep-ph].
[17] Kirill Tuchin, "Electromagnetic field and the chiral magnetic effect in the quark-gluon plasma," Phys. Rev. **C91**, 064902 (2015), arXiv:1411.1363 [hep-ph].
[18] M. Mace, S. Schlichting, and R. Venugopalan, "Off-equilibrium sphaleron transitions in the glasma," Phys. Rev. **D93**, 074036 (2016), arXiv:1601.07342 [hep-ph].
[19] B. I. Abelev et al. (STAR), "Azimuthal Charged-Particle Correlations and Possible Local Strong Parity Violation," Phys. Rev. Lett. **103**, 251601 (2009), arXiv:0909.1739 [nucl-ex].
[20] B. I. Abelev et al. (STAR), "Observation of charge-dependent azimuthal correlations and possible local strong parity violation in heavy ion collisions," Phys. Rev. **C81**, 054908 (2010), arXiv:0909.1717 [nucl-ex].
[21] L. Adamczyk et al. (STAR), "Fluctuations of charge separation perpendicular to the event plane and local parity violation in $\sqrt{s_{NN}}$ = 200 GeV Au+Au collisions at the BNL Relativistic Heavy Ion Collider," Phys. Rev. **C88**, 064911 (2013), arXiv:1302.3802 [nucl-ex].
[22] L. Adamczyk et al. (STAR), "Measurement of charge multiplicity asymmetry correlations in high-energy nucleus-nucleus collisions at $\sqrt{s_{NN}}$ = 200 GeV," Phys. Rev. **C89**, 044908 (2014), arXiv:1303.0901 [nucl-ex].
[23] L. Adamczyk et al. (STAR), "Beam-energy dependence of charge separation along the magnetic field in Au+Au collisions at RHIC," Phys. Rev. Lett. **113**, 052302 (2014), arXiv:1404.1433 [nucl-ex].
[24] Betty Abelev et al. (ALICE), "Charge separation relative to the reaction plane in Pb-Pb collisions at $\sqrt{s_{NN}}$ = 2.76 TeV," Phys. Rev. Lett. **110**, 012301 (2013), arXiv:1207.0900 [nucl-ex].
[25] Vardan Khachatryan et al. (CMS), "Observation of charge-dependent azimuthal correlations in p-Pb collisions and its implication for the search for the chiral magnetic effect," Phys. Rev. Lett. **118**, 122301 (2017), arXiv:1610.00263 [nucl-ex].
[26] Shreyasi Acharya et al. (ALICE), "Constraining the magnitude of the Chiral Magnetic Effect with Event Shape Engineering in Pb-Pb collisions at $\sqrt{s_{\rm NN}}$ = 2.76 TeV," Phys. Lett. **B777**, 151–162 (2018), arXiv:1709.04723 [nucl-ex].
[27] Albert M. Sirunyan et al. (CMS), "Constraints on the chiral magnetic effect using charge-dependent azimuthal correlations in pPb and PbPb collisions at the CERN Large Hadron Collider," Phys. Rev. **C97**, 044912 (2018), arXiv:1708.01602 [nucl-ex].
[28] Sergei A. Voloshin, "Parity violation in hot QCD: How to detect it," Phys. Rev. **C70**, 057901 (2004), arXiv:hep-ph/0406311 [hep-ph].
[29] Masayuki Asakawa, Abhijit Majumder, and Berndt Muller, "Electric Charge Separation in Strong Transient Magnetic Fields," Phys. Rev. **C81**, 064912 (2010), arXiv:1003.2436 [hep-ph].
[30] Adam Bzdak, Volker Koch, and Jinfeng Liao, "Azimuthal correlations from transverse momentum conservation and possible local parity violation," Phys. Rev. C **83**, 014905 (2011), arXiv:1008.4919 [nucl-th].
[31] Berndt Muller and Andreas Schafer, "Charge Fluctuations from the Chiral Magnetic Effect in Nuclear Collisions," Phys. Rev. C **82**, 057902 (2010), arXiv:1009.1053 [hep-ph].
[32] Fuqiang Wang, "Effects of Cluster Particle Correlations on Local Parity Violation Observables," Phys. Rev. **C81**, 064902 (2010), arXiv:0911.1482 [nucl-ex].
[33] Soren Schlichting and Scott Pratt, "Explaining Angular Correlations Observed at RHIC with Flow and Local Charge Conservation," (2010), arXiv:1005.5341 [nucl-th].
[34] Guo-Liang Ma and Bin Zhang, "Effects of final state interactions on charge separation in relativistic heavy ion collisions," Phys. Lett. **B700**, 39–43 (2011), arXiv:1101.1701 [nucl-th].
[35] Yifeng Sun and Che Ming Ko, "Chiral kinetic approach to the chiral magnetic effect in isobaric collisions," Phys. Rev. **C98**, 014911 (2018), arXiv:1803.06043 [nucl-th].
[36] Niseem Magdy, Shuzhe Shi, Jinfeng Liao, N. Ajitanand, and Roy A. Lacey, "New correlator to detect and characterize the chiral magnetic effect," Phys. Rev. **C97**, 061901 (2018), arXiv:1710.01717 [physics.data-an].
[37] Niseem Magdy, Shuzhe Shi, Jinfeng Liao, Peifeng Liu, and Roy A. Lacey, "Examination of the observability of a chiral magnetically driven charge-separation difference in collisions of the $^{96}_{44}$Ru + $^{96}_{44}$Ru and $^{96}_{40}$Zr + $^{96}_{40}$Zr isobars at energies available at the BNL Relativistic Heavy Ion Collider," Phys. Rev. **C98**, 061902 (2018), arXiv:1803.02416 [nucl-ex].
[38] E. G. Judd et al., "The evolution of the STAR Trigger System," Nucl. Instrum. Meth. **A902**, 228–237 (2018).
[39] M. Anderson et al., "The Star time projection chamber: a unique tool for studying high multiplicity events at RHIC," Nucl. Instrum. Meth. **A499**, 659–678 (2003), arXiv:nucl-ex/0301015 [nucl-ex].
[40] L. Adamczyk et al. (STAR), "Inclusive charged hadron elliptic flow in Au + Au collisions at $\sqrt{s_{NN}}$ = 7.7 - 39 GeV," Phys. Rev. **C86**, 054908 (2012), arXiv:1206.5528 [nucl-ex].
[41] Piotr Bozek, "Azimuthal angle dependence of the charge imbalance from charge conservation effects," Phys. Rev. **C97**, 034907 (2018), arXiv:1711.02563 [nucl-th].
[42] L. Adamczyk et al. (STAR), "Measurement of elliptic flow of light nuclei at $\sqrt{s_{NN}}$ = 200, 62.4, 39, 27, 19.6, 11.5, and 7.7 GeV at the BNL Relativistic Heavy Ion Collider," Phys. Rev. **C94**, 034908 (2016), arXiv:1601.07052 [nucl-ex].
[43] Zi-Wei Lin, Che Ming Ko, Bao-An Li, Bin Zhang, and Subrata Pal, "A Multi-phase transport model for relativistic heavy ion collisions," Phys. Rev. **C72**, 064901 (2005), arXiv:nucl-th/0411110 [nucl-th].
[44] Jurgen Schukraft, Anthony Timmins, and Sergei A. Voloshin, "Ultra-relativistic nuclear collisions: event shape engineering," Phys. Lett. **B719**, 394–398 (2013), arXiv:1208.4563 [nucl-ex].
[45] Jie Zhao, "Search for the chiral mag-

netic effect in relativistic heavy-ion collisions," Int. J. Mod. Phys. **A33**, 1830010 (2018), arXiv:1805.02814 [nucl-ex].
[46] Ling Huang, Mao-Wu Nie, and Guo-Liang Ma, "Sensitivity analysis for observables of the chiral magnetic effect using a multiphase transport model," Phys. Rev. C **101**, 024916 (2020), arXiv:1906.11631 [nucl-th].